

# Coherent structures and spectral shapes of kinetic Alfvén wave turbulence in solar wind at 1 AU

Hemam Dinesh Singh and Bheem Singh Jatav

Department of Physics, Sikkim University, Gangtok, Sikkim, 737102, India; [hemamdine@gmail.com](mailto:hemamdine@gmail.com)

Received 2018 December 1; accepted 2019 January 4

**Abstract** This paper presents the generation of kinetic Alfvén wave (KAW) coherent structures of magnetic filaments applicable to solar wind at 1 AU, when the background plasma density is modified by parallel ponderomotive force and Joule heating. The inhomogeneity in the magnetic field, which was included as a perturbation in the transverse direction of the magnetic field, takes energy from the main pump KAWs and generates the filamentary structures. When the intensity is high enough, the filaments are broken down and the energy initially confined to low wavenumbers is redistributed to higher wavenumbers, leading to cascades of energy at small scales less than the ion acoustic gyroradius or comparable to electron gyroradius. The magnetic field spectral profile is generated from the numerical simulation results, and its dependence on different directions of the wavevector and initial conditions of the simulation representing the transverse magnetic field inhomogeneity is studied. The relevance of these results with other spacecraft observations and measurements is also pointed out.

**Key words:** plasmas — turbulence — waves — solar wind

## 1 INTRODUCTION

In a magnetized plasma, Alfvén waves are produced by the restoring force coming from the magnetic tension while the ion mass provides the inertia to maintain the wave. Kinetic Alfvén waves (KAWs) are low frequency (compared to ion cyclotron frequency), dispersive, shear Alfvén modes that exist when their perpendicular wavelength is comparable to either the ion gyroradius or the electron inertial length, while the parallel wavelengths are longer than the ion inertial length (here, the perpendicular (parallel) direction means transverse (along) to the ambient (background) magnetic field direction). Their plasma  $\beta$  is in the intermediate range ( $m_e/m_i \ll \beta \ll 1$ ), where  $\beta = 8\pi n_0 T/B_0^2$  (thermal to magnetic pressure ratio),  $n_0$  is the unperturbed plasma number density,  $T(= T_e \approx T_i)$  is the plasma temperature,  $B_0$  is the external ambient direct current (DC) magnetic field and  $m_e/m_i$  is the electron to ion mass ratio. In this plasma  $\beta$  regime, the electron thermal speed exceeds the Alfvén speed, thereby allowing the electrons to move fast enough to respond to any adiabatic changes in density or field profile.

Many studies (Li et al. 2016; Tu & Marsch 1993; Bavassano et al. 1998; Neugebauer 2004) have shown that the Alfvénicity measured by the correlation of the field and velocity components decreases with solar distances. At a solar distance of 0.3 AU, an Alfvénicity of around 3 was found (Tu et al. 1990; Marsch & Tu 1990). At a solar distance of 1 AU, it becomes around less than 0.7 (Tu & Marsch 1995) showing that as the solar wind expands, the plasma becomes magnetically dominated. However, Wang et al. (2012) pointed out the existence of large-amplitude Alfvén waves near 1 AU, with an Alfvénicity of around 1. There are many independent observational evidences showing the existence of KAWs in the solar wind in the form of KAW turbulence at 1 AU and perhaps throughout of the heliosphere (Podesta 2013; Howes et al. 2006, 2008b,c, 2011b; Schekochihin et al. 2008, 2009; Boldyrev & Perez 2012).

KAWs develop field aligned electric fields which can lead to the acceleration and heating of the charged particles along the magnetic field direction (Hasegawa & Chen 1975; Wu 2003; Wu & Chao 2004), thus producing anisotropic and mass-dependent energization of heavy

ions (Voitenko & Goossens 2004; Wu & Yang 2006). The existence of KAWs is evident from measurements by the *Polar* spacecraft in the magnetotail region (Wygant et al. 2002) and inner magnetosphere at  $6.6R_E$  (Sergeev et al. 2000). Observations from the Ultraviolet Coronagraph Spectrometer (UVCS) on board *Solar and Heliospheric Observatory (SOHO)* demonstrated the existence of KAWs in the inner heliosphere (Cranmer et al. 1999; Marsch & Tu 2001). Therefore, the study of KAWs plays a significant role in understanding the various phenomena happening in space and laboratory plasmas, such as solar wind turbulence (Chaston et al. 2005a), coronal heating (Wu & Fang 2003) and auroral particle acceleration (Wygant et al. 2002; Chaston et al. 2003, 2004, 2005b).

From the analysis of *Polar* spacecraft data, Wygant et al. (2002) found coherent structures of KAWs with perpendicular scale size comparable to ion gyro radius and having a large characteristic ratio between the amplitudes of electric and magnetic field fluctuations. Many observations and investigations related to the generation of KAWs suggested that these coherent structures are associated with inhomogeneities in magnetic fields, densities and temperatures (Chen & Liu 1976; Lee et al. 1994; Xu et al. 2008). Because of these magnetic field fluctuations and the fact that the ponderomotive force arises from the nonlinear magnetic pressure (because of a non-zero spatial gradient in plasma density and temperature), KAWs generate the coherent structures or filaments in the high magnetic field intensity parallel to the ambient field. As the KAW propagates, these magnetic field structures are broken down and the energy is redistributed to other higher wavenumbers, leading to heating of the plasma.

The injection of KAW energy at ion/proton gyro-scales and the dissipation of this energy at electron inertial scales, producing plasma turbulence in solar and magnetospheric plasmas, are widely observed (Howes et al. 2008a; Sahraoui et al. 2009, 2010). These turbulent processes are generated mainly by the nonlinear wave-wave or wave-particle interactions, or Landau damping in the plasma. The solar wind, which permeates throughout the heliosphere, acts as a laboratory for theoretical and observational studies, because they are fully developed by space plasma turbulence (Bruno & Carbone 2013). In the last few years, high time resolution magnetic field measurements by many space missions, such as *Advanced Composition Explorer (ACE)*, *Acceleration, Reconnection, Turbulence and Electrodynamics of the Moon's Interaction with the Sun (ARTEMIS)* and *Cluster* spacecrafts, have enhanced

the ongoing research on space plasma turbulence at kinetic scales.

It is widely accepted that the fluctuating magnetic field power spectra in the magnetohydrodynamic (MHD) region approximately follow the Kolmogorov index of  $-5/3$  ( $\propto k^{-5/3}$ ) in the inertial range (Matthaeus et al. 1982; Horbury et al. 1996; Leamon et al. 1998; Bale et al. 2005). After this range, the first break in the spectral scale appears at the ion gyroradius or the ion inertial length, giving a steeper scaling of around  $-2.5$ , known as the dispersion range (Alexandrova et al. 2008; Chen et al. 2014). The second break in the spectral index occurs when it is less than the ion scales up to the electron scales, leading to steeper slopes of about  $-5$  to  $-3$  known as dissipation or sub-ion range (Alexandrova et al. 2009; Sahraoui et al. 2010; Howes et al. 2011a; Chang et al. 2013). In between these two breaks, there is a transition region having the variable spectral slope of  $-4$  to  $-2$  (Leamon et al. 1998; Smith et al. 2006; Roberts et al. 2013) or no properly defined spectral index (Bruno & Trenchi 2014). The steeper spectral slope in the transition region could be contributed due to the dissipation producing exponential spectral slope (Alexandrova et al. 2012) or due to plasma coherent structures (Lion et al. 2016). Sahraoui et al. (2013), analyzing *Cluster* spacecraft data, found another wide range of spectral slopes ranging from  $-5.5$  to  $-3.5$ , suggesting a lack of generality in the nature of turbulent fluctuations at smaller scales, i.e. at electron scale dissipation region.

There are numerous studies which have tried to understand the physics behind steepening of the spectral index (Markovskii et al. 2008; Perri et al. 2010; Bruno & Trenchi 2014). However, there is no generally accepted mechanism or process that can explain it till now, leaving it as an unsolved problem. It is generally accepted that the local cascade of magnetic energy fluctuations from large to smaller scales causes solar wind turbulence. Two leading hypotheses to explain the nature of the solar wind turbulence fluctuations in the dissipation range are the fluctuations having the characteristic scales of either KAWs (Leamon et al. 2000; Howes et al. 2008b; Schekochihin et al. 2009) or whistler waves (Galtier 2006; Gary & Smith 2009; Saito et al. 2010; Podesta et al. 2010; Shaikh 2010). Other possibilities are ion cyclotron waves (Goldstein et al. 1994; Leamon et al. 1998; Gary 1999; He et al. 2011), ion Bernstein waves (Howes 2009; Sahraoui et al. 2012) and current sheets (Sundkvist et al. 2007; Osman et al. 2011). The nonlinear interaction of inward and outward Alfvén waves can generate Alfvénic turbulence in the chromosphere as analyzed by Liu et al. (2014) from satellite data

to understand the nature of chromospheric turbulence as well as chromospheric heating. Lion et al. (2016) investigated the process leading to a sharp spectral break in the transition region and sub-ion scales using in-situ data from the *Wind* spacecraft. They showed that the presence of large amplitude Alfvénic coherent structures (vortex-like) and current sheets is also a possible mechanism for spectral break and steepening. KAWs can distribute the energy at sub-ion scales with  $\omega < \omega_{ci}$ , but they cannot cascade the energy via turbulence down to electron scales. At this scale, the whistler mode ( $\omega > \omega_{ci}$ ) is more relevant.

The KAWs can be generated or excited by many plasma instabilities, such as the kinetic fire-hose instability driven by the ion and electron temperature anisotropy (Yoon 1995; Malovichko 2008; Chen & Wu 2010), the field aligned current instability (Chen et al. 2011, 2013a; Chen & Wu 2012), velocity shear instability (Siversky et al. 2005; Duan et al. 2012) and the diamagnetic drift instability driven by inhomogeneities in density and magnetic field (Duan & Li 2005; Duan et al. 2005). In fact, magnetic coherent structures or filaments are the manifestation of field-aligned density irregularities (perturbations) in the plasma. The interaction between KAWs and filament structures with density fluctuations in a transverse inhomogeneous plasma has been investigated by many authors (Tsiklauri 2011, 2012; Chen et al. 2015; Wu & Chen 2013). Tsiklauri (2011, 2012) used particle in cell simulations in 2.5D and 3D fully kinetic regimes to model the coronal heating when the inhomogeneity in density is produced by the solar flares triggering the KAWs. The results indicate that the electrons are effectively accelerated by the parallel electric field generated only in the regions where density inhomogeneity occurs (i.e., at the coronal loop edges) and the ions are heated effectively in the direction transverse to the magnetic field by the perpendicular electric fields caused by the KAWs. A similar electron acceleration mechanism has also been found in Earth's magnetosphere. Tsiklauri (2011); Chen et al. (2015) demonstrated that density perturbation with an inhomogeneous density gradient results in KAW instability such that both the real frequency and growth rate are dependent on the transverse spatial position. Wu & Chen (2013) also investigated the instability of KAWs driven by transverse density gradient and showed that the instability experiences its maximal growth rate at the perpendicular wavelength close to the spatial characteristic scale of the density gradient. The transverse density fluctuations always occur with KAWs because of their strong anisotropy (with the perpendicular wavelengths being much shorter than parallel ones) and coupling with

strong electrostatic modes. Sahraoui et al. (2010) investigated the spectrum of turbulence and showed that highly oblique KAWs are responsible for strong anisotropy.

The main aim of this present paper is to investigate steady state KAW dynamics to understand the dependence of initial plasma inhomogeneities on coherent plasma structure generation and cascade of energy at different wavevectors. This paper is organized as follows: The KAW dynamics applicable to solar wind at 1 AU are described in Section 2. In Section 3, we present the numerical simulations and results leading to the generation of coherent structures that are aligned to the magnetic field and spectral energy fluctuations in Fourier space, and their spectral indices. Finally, Section 4 summarizes our findings and gives conclusions.

## 2 MODEL KAW DYNAMICS

The dynamical equation of low frequency KAWs in the intermediate  $-\beta$  regime ( $m_e/m_i \ll \beta \ll 1$ ), propagating in the  $x-z$  plane ( $\mathbf{k}_0 = k_{0x}\hat{x} + k_{0z}\hat{z}$ ) with ambient DC magnetic field  $B_0$  along the  $z$ -axis ( $\mathbf{B}_0 = B_0\hat{z}$ ), is obtained by the two-fluid approach and applying the procedure of linearization. The parameters of the medium, such as density, velocity and electromagnetic fields, are separated into two parts: an equilibrium (undisturbed) part indicated by the subscript 0 and a superimposed disturbance (perturbation) part denoted by the subscript 1.

$$\begin{aligned} n &= n_0 + n_1, \\ \mathbf{v} &= \mathbf{v}_0 + \mathbf{v}_1, \\ \mathbf{E} &= \mathbf{E}_0 + \mathbf{E}_1, \\ \mathbf{B} &= \mathbf{B}_0 + \mathbf{B}_1. \end{aligned} \quad (1)$$

The equilibrium plasma has constant and uniform  $n_0$  and  $\mathbf{B}_0$  with zero  $\mathbf{E}_0$  and  $\mathbf{v}_0$ .

$$\nabla n_0 = \mathbf{v}_0 = \mathbf{E}_0 = 0, \quad (2)$$

$$\frac{\partial n_0}{\partial t} = \frac{\partial \mathbf{v}_0}{\partial t} = \frac{\partial \mathbf{E}_0}{\partial t} = 0. \quad (3)$$

In the linearization process, the terms containing the higher powers of the perturbing amplitude factors can be neglected. Equation of motion

$$\frac{\partial \mathbf{v}_{j1}}{\partial t} \approx \frac{q_j}{m_j} \mathbf{E}_1 + \frac{q_j}{cm_j} (\mathbf{v}_{j1} \times \mathbf{B}_0) - \frac{\gamma_j k_B T_j}{n_{j0} m_j} \nabla n_{j1}. \quad (4)$$

Continuity equation

$$\frac{\partial n_{j1}}{\partial t} + n_{j0} \nabla \cdot \mathbf{v}_{j1} \approx 0. \quad (5)$$

Faraday's law

$$\nabla \times \mathbf{E}_1 = -\frac{1}{c} \frac{\partial \mathbf{B}_1}{\partial t}, \quad (6)$$

where the subscript  $j$  assumes values of  $e$  and  $i$  for electrons and ions respectively,  $v$  is the velocity,  $q$  is the charge,  $m$  is the mass,  $c$  is the speed of light in a vacuum,  $\gamma$  is the ratio of the specific heats  $c_p/c_v$ ,  $k_B$  is the Boltzmann constant, and  $n$  is the plasma number density satisfying the quasineutrality condition, i.e.,  $n_{e0} \simeq n_{i0} \simeq n_0$  and  $n_{e1} \simeq n_{i1} \simeq n_1$ . Here we assume the electrons and ions to be isothermal, i.e.,  $\gamma_e = \gamma_i = 1$ .

From Equation (4), the perpendicular components of the electron and ion fluid velocities in the low frequency KAWs ( $\omega \ll \omega_{ci}$  and  $\omega \ll \omega_{ce}$ ) are given by, respectively,

$$(\mathbf{v}_{e1})_{\perp} \approx \frac{c}{B_0} \mathbf{E}_{1\perp} \times \hat{z} - \frac{k_B T_e}{m_e \omega_{ce} n_0} \hat{z} \times \nabla_{\perp} n_1, \quad (7)$$

$$\begin{aligned} (\mathbf{v}_{i1})_{\perp} \approx & \frac{e}{\omega_{ci} m_i} \left[ \mathbf{E}_{1\perp} - \frac{k_B T_i}{en_0} \nabla_{\perp} n_1 \right] \times \hat{z} \\ & - \frac{i\omega}{\omega_{ci}^2} \frac{e}{m_i} \left[ \mathbf{E}_{1\perp} - \frac{k_B T_i}{en_0} \nabla_{\perp} n_1 \right], \end{aligned} \quad (8)$$

and the time derivative of the parallel electron velocity is

$$\frac{\partial (\mathbf{v}_{e1})_z}{\partial t} = \frac{-eE_{1z}}{m_e} - \frac{k_B T_e}{m_e n_0} \frac{\partial n_1}{\partial z}. \quad (9)$$

The current density is written as

$$\mathbf{J} \approx en_0 (\mathbf{v}_{i1} - \mathbf{v}_{e1}). \quad (10)$$

Here  $\omega$  is the frequency of the KAW,  $\omega_{ce} (= eB_0/m_e c)$  is the electron cyclotron frequency and  $\omega_{ci} (= eB_0/m_i c)$  is the ion cyclotron frequency.

Hereafter, we will drop the subscript "1" in the varying quantities of  $\mathbf{v}$ ,  $\mathbf{E}$  and  $\mathbf{B}$  (except in  $n$ ) with the understanding that they represent the disturbed (perturbed) part.

Writing the  $y$ -component of Faraday's law for KAWs propagating in the  $x-z$  plane, we get

$$\frac{1}{c} \frac{\partial B_y}{\partial t} = \frac{\partial E_z}{\partial x} - \frac{\partial E_x}{\partial z}. \quad (11)$$

Using the conservation of current density,  $\nabla \cdot \mathbf{J} = 0$ , and also by taking  $J_z \approx -en_0 v_{ez}$  and  $\mathbf{J}_{\perp} \approx en_0 (\mathbf{v}_{i\perp} - \mathbf{v}_{e\perp})$ , we arrive at

$$\frac{\partial^2 E_x}{\partial x \partial t} = \frac{B_0 \omega_{ci}}{c} \left( \frac{\partial v_{ez}}{\partial z} \right). \quad (12)$$

Taking the  $z$ -component of Ampere's law and eliminating the parallel component of current density, and substituting it in Equation (12), yields,

$$\frac{\partial E_x}{\partial t} = -\frac{v_A^2}{c} \left( 1 - \frac{n_1}{n_0} \right) \frac{\partial B_y}{\partial z}, \quad (13)$$

where  $v_A (= \sqrt{B_0^2/4\pi n_0 m_i})$  is the Alfvén wave speed.

Now we can find the time derivatives of parallel electric field from the parallel component of Ampere's law and substituting therein the parallel electron fluid velocity given by Equation (9) and the continuity Equation (5) as

$$\frac{\partial E_z}{\partial t} = -\frac{v_{te}^2 \lambda_e^2}{c} \frac{\partial}{\partial x} \frac{\partial^2 B_y}{\partial z^2}, \quad (14)$$

where  $\lambda_e (= c/\omega_{pe})$  is the electron collisionless skin depth (electron inertial length),  $\omega_{pe} (= \sqrt{4\pi n_0 e^2/m_e})$  is the electron plasma oscillation frequency and  $v_{te} (= \sqrt{\frac{k_B T_e}{m_e}})$  is the electron thermal speed.

Differentiating Equation (11) with respect to time and substituting therein the  $z$ -derivative of Equation (13) and the  $x$ -derivative of Equation (14), we produce the dynamical equation for intermediate plasma  $-\beta$ , low frequency ( $\omega \ll \omega_{ci}$ ) KAWs propagating in the  $x-z$  plane as (Hasegawa & Chen 1975; Bellan & Stasiewicz 1998; Shukla et al. 1999; Shukla & Stenflo 2000a)

$$\frac{\partial^2 B_y}{\partial t^2} = -v_A^2 \rho_s^2 \frac{\partial^4 B_y}{\partial x^2 \partial z^2} + v_A^2 \left( 1 - \frac{n_1}{n_0} \right) \frac{\partial^2 B_y}{\partial z^2}, \quad (15)$$

where  $\rho_s (= \lambda_e v_{te}/v_A = c_s/\omega_{ci})$  is the ion acoustic gyro-radius at the electron temperature and  $c_s (= \sqrt{k_B T_e/m_i})$  is the ion sound speed.

The dispersion relation of KAWs for intermediate plasma- $\beta$  (Shukla & Stenflo 2005) can be recovered from Equation (15) by taking the Fourier Transform as

$$\frac{\omega^2}{k_{0z}^2 v_A^2} = 1 + k_{0x}^2 \rho_s^2. \quad (16)$$

The dynamical equation, Equation (15), is satisfied by the perturbed KAW fields. At the same time it is also satisfied for the KAW, which is a plane wave at which a nonuniform perturbation is superimposed, as is the case here.

Here, we consider plane polarized KAWs with base frequency  $\omega$  modulated by a slowly varying envelope  $B'_y(x, z)$ . Let us assume the envelope solution for Equation (15) in the form of a plane wave as

$$B_y = B'_y(x, z) e^{i(k_{0x}x + k_{0z}z - \omega t)}. \quad (17)$$

$B'_y(x, z)$  is the perpendicular component of the KAW magnetic field that has slowly varying amplitude in space in comparison to the exponential part  $e^{i(k_{0x}x + k_{0z}z)}$ . Substituting it in Equation (15), one gets the dynamical equation in steady state as

$$\begin{aligned} i \frac{2}{k_{0z}} \frac{\partial B'_y}{\partial z} + \rho_s^2 \frac{k_{0x}^2}{k_{0z}^2} \frac{\partial^2 B'_y}{\partial z^2} + \rho_s^2 \frac{\partial^2 B'_y}{\partial x^2} \\ + 2ik_{0x} \rho_s^2 \frac{\partial B'_y}{\partial x} + \frac{n_1}{n_0} B'_y = 0. \end{aligned} \quad (18)$$

In an inhomogeneous plasma, if there is spatial variation in the amplitudes of the KAWs, a force known as the ponderomotive force arising from the nonlinear magnetic-gradient acts upon the plasma. This ponderomotive force combined with the electron Joule heating (Shukla & Stenflo 1999) can modify the density. In laboratory and space plasmas, magnetic field aligned density humps and cavities associated with large amplitude KAWs were reported (Gekelman et al. 1999).

The perturbation in electron or ion density to the background plasma in adiabatic response (slow variation in time with respect to density fluctuations) was found as (Shukla & Stenflo 2000b)

$$n_1 \approx n_0 \left( e^{\xi |B'_y|^2} - 1 \right), \quad (19)$$

where  $\xi = \{[1 - \Delta(1 + \delta)v_A^2 k_{0z}]/16\pi n_0 T_e \omega^2\}$ ,  $\Delta = \omega^2/\omega_{ci}^2$  and  $\delta = m_e k_{0x}^2/m_i k_{0z}^2$ . For  $\omega(1 + \delta)^{1/2} < \omega_{ci}$ , the change in the magnetic field aligned quasi-stationary density is a hump. Since the plasma  $\beta \gg m_e/m_i$  was considered, the ion and electron thermal speeds exceed the Alfvén wave speed, thereby allowing the electrons or ions to move fast enough to respond to any adiabatic response in density.

Using Equation (19), we rewrite Equation (18) in dimensionless form as

$$i \frac{\partial B'_y}{\partial z} + 2iK \frac{\partial B'_y}{\partial x} + K^2 \frac{\partial^2 B'_y}{\partial z^2} + \frac{\partial^2 B'_y}{\partial x^2} + \frac{1}{2g} \left( e^{2g|B'_y|^2} - 1 \right) B'_y = 0, \quad (20)$$

where  $K = k_{0x}\rho_s$  is a dimensionless parameter. It is the transverse wavenumber normalized to the inverse of the ion acoustic gyroradius  $\rho_s$  at electron temperature. Here, we have introduced the dimensionless parameter  $g$  for the sake of generality. It can also govern the amplitude of the pump KAW. When  $g = 0$ , it leads to the well known quadratic nonlinearity. Hence, the coupling to the density perturbation and magnetic field is in some way controlled by this parameter. The normalizing parameters are  $z_n = 2/k_{0z}$ ,  $x_n = \rho_s$  and  $B_n = [\{1 - \Delta(1 + \delta)\}V_A^2 k_{0z}^2/16\pi n_0 T_e \omega^2]^{-1/2}$ .

When  $g = 0$ , the density profile becomes quadratic in the magnetic field and Equation (20) takes the form of a cubic nonlinear Schrödinger (NLS) type equation. On the other hand, as  $g$  becomes non-zero, Equation (20) is no longer integrable and may lead to spatial chaos.

By considering  $K = 0$  and a simpler homogeneous solution of Equation (20) as  $B_{y0}e^{-iz}$  (Zhou et al. 1992; Zhou & He 1994), we could find the relation between the

initial KAW pump wave amplitude and the parameter  $g$  as

$$|B_{y0}| = \sqrt{\frac{\ln|1 - 2g|}{2g}}, \quad (21)$$

where  $B_{y0}$  is the amplitude of the homogeneously pumped KAW and the range of  $g$  is  $0 \leq g < 1/2$ .

In the following section we will solve Equation (20) numerically when the main KAW assumes the form of a plain/Gaussian wavefront with different types of perturbations.

### 3 NUMERICAL SIMULATION AND RESULTS

We carried out the numerical simulation of Equation (20) by applying the following four initial conditions to understand the dependence of the initial conditions of the inhomogeneous magnetic field on the generation of Alfvénic coherent structures. The first initial condition (IC-1) is a uniform plane KAW with fixed amplitude and a sinusoidal periodic perturbation superimposed on it, given as

$$B'_y(x, 0) = B_{y0}[1 + \varepsilon \cos(\alpha_x x)] \quad (\text{IC-1})$$

where  $\varepsilon$  and  $\alpha_x$  (normalized by  $x_n^{-1}$ ) are the magnitude and wavenumber of the perturbation respectively.

The second initial condition (IC-2) is a Gaussian perturbation superimposed on a uniform plain KAW and expressed as

$$B'_y(x, 0) = B_{y0}[1 + \varepsilon \exp(-x^2/r_{01}^2)], \quad (\text{IC-2})$$

where  $r_{01}$  (normalized by  $x_n$ ) is the transverse scale size of the perturbation.

The third initial condition (IC-3) is a sinusoidal perturbation superimposed on a non-uniform KAW of a Gaussian wave front

$$B'_y(x, 0) = B_{y0}[\exp(-x^2/r_0^2) + \varepsilon \cos(\alpha_x x)], \quad (\text{IC-3})$$

where  $r_0$  (normalized by  $x_n$ ) is the transverse scale size of the main KAW initial beam width.

The fourth initial condition (IC-4) is a random perturbation superimposed on the Gaussian wavefront

$$B'_y(x, 0) = B_{y0}[\exp(-x^2/r_0^2) + \varepsilon \exp(2\pi i\theta(x))], \quad (\text{IC-4})$$

where  $\theta(x)$  is a random variable uniformly distributed in  $[0, 1]$ .

The numerical code was written in FORTRAN using the technique of pseudo-spectral method with Fast Fourier Transform (FFT) for transverse ( $x$ -direction) space integration with periodic length  $L_x = 2\pi/\alpha_x$ , implementing  $2^8$  grid points and a finite-difference method with a

predictor-corrector scheme for propagation along the  $z$ -direction and a small step size  $dz = 5 \times 10^{-5}$ . The linear terms (second, third and fourth terms in the equation) were solved in Fourier space and the nonlinear term (fifth term) was solved by taking the local product in real space first and then performing the FFT to transform into  $k$ -space. The numerical algorithm was written first for the well-known cubic NLS equation which was obtained in our case by applying  $K = 0$  and  $g = 0$ , i.e., the density profile becoming quadratic with respect to magnetic field,  $n_1/n_0 \simeq \xi|B'_y|^2$ . The cubic NLS equation is integrable and this constant of integration was checked in our simulation by computing the plasmon number  $N = \sum_k |B_k|^2$  (the conservation of wave energy). We found this number remained constant up to the precision of six decimal places throughout the computation. After fully testing this algorithm, we modified it for solving our present equation.

In the numerical simulation, we used  $\varepsilon = 0.1$ ,  $\alpha_x = 0.5$ ,  $r_0 = 1.0$ ,  $r_{01} = 5$ , giving  $L_x = 2\pi/\alpha_x \simeq 12.5 \simeq 2.5r_{01}$ . We chose  $g = 0.01$ , thereby producing  $B_{y0} \simeq 1.005$  and the magnetic fluctuation  $|\delta B_y/B_{y0}| \simeq 0.1$ . Many observations from the satellites reported strong depressions of magnetic field,  $\delta B/B_0 \sim 90\%$ , in the cusp region of the magnetosphere, magnetosheath, magnetopause region (Tsurutani et al. 1982; Savin et al. 1998) and solar wind (Winterhalter et al. 1994).

Further, to calculate the other parameter values for the simulation and related applications, solar wind data measured at 1 AU by the *Helios 2* spacecraft (Cravens 2004) were used:  $B_0 \approx 1 \times 10^{-4}$  G,  $n_0 \approx 5 \text{ cm}^{-3}$ ,  $T_e \approx 0.5 \times 10^5$  K = 4.31 eV and  $T_i \approx 0.2 \times 10^5$  K = 1.72 eV. Accordingly we found  $\beta = 0.121$ ,  $v_{te} \approx 8.7 \times 10^7 \text{ cm s}^{-1}$ ,  $V_A \approx 9.8 \times 10^6 \text{ cm s}^{-1}$  and  $\omega_{ci} \approx 0.95 \text{ rad s}^{-1}$ .  $\rho_s = 2.5 \times 10^6 \text{ cm}$ ,  $\rho_i = (\sqrt{T_i/T_e})\rho_s = 3.75 \times 10^6 \text{ cm}$ ,  $\rho_e = 4.9 \times 10^4 \text{ cm}$ ,  $\lambda_i = 9.9 \times 10^6 \text{ cm}$  and  $\lambda_e = 2.38 \times 10^5 \text{ cm}$ . Here, the previously undefined parameters are ion gyroradius  $\rho_i (= v_{ti}/\omega_{ci})$ , electron gyroradius  $\rho_e (= v_{te}/\omega_{ce})$ , ion inertial length (or ion skin depth)  $\lambda_i = c/\omega_{pi}$  and ion plasma oscillation frequency  $\omega_{pi} (= \sqrt{4\pi n_0 e^2/m_i})$ .

For  $\omega = 0.01 \text{ rad s}^{-1}$  and  $K = k_{0x}\rho_s = 0.01$ , we get  $k_{0z} = 6.44 \times 10^{-9} \text{ cm}^{-1}$  and  $k_{0x} = 3.98 \times 10^{-9} \text{ cm}^{-1}$ . The values of other normalizing parameters are  $B_n \simeq 4.2 \times 10^{-5}$  G,  $x_n \simeq 2 \times 10^6 \text{ cm}$  and  $z_n \simeq 3 \times 10^8 \text{ cm}$ .

Now we present the numerical simulation results by taking four initial conditions: IC-1, IC-2, IC-3 and IC-4 as defined earlier. The spatial evolution of KAW packets in 2D are displayed in Figure 1(a)–1(d) for four kinds of initial conditions. It is evident from the figures that the coherent structures or filaments of KAWs are localized in space

covering all scales from the energy injection scale (when the size of a filament is comparable to ion gyroradius/ion inertial length) to dissipation scale (when the size of a filament is comparable to electron gyroradius/electron inertial length). In the case of IC-1 and IC-2, the pattern of filament formation is almost the same, reaching the peak intensity  $|B_y|^2 = 12.29$  at around  $z = 31.50$  and  $x = 0.29$  for IC-1, and  $|B_y|^2 = 14.17$  at around  $z = 31$  and  $x = 0.40$  for IC-2. Most of the filaments are formed at the middle of the system length  $L_x$  and a few more in the boundary. In the case of IC-3 and IC-4, the magnetic field intensities for filaments are very low in comparison to those for IC-1 and IC-2. The peak intensity of 0.96 is found at  $x = 6.18$  and  $z = 12.50$  for IC-3. The same values are also observed for IC-4. In case of IC-3 and IC-4, the filaments are already distributed in the transverse direction initially from  $z = 0$ .

To understand the generation of magnetic coherent structures, we can make an analogy with laser focusing studied by Krueer (2003). In the presence of background density perturbations, the dielectric constant of the medium will be modified, and hence change the refractive index. A laser beam propagating through a medium with varying refractive index will act as a focusing lens and focuses the wave. In our case, the parallel ponderomotive force will initiate perturbations in the density. When the KAWs propagate through this medium, their phase velocity will change and produce the localization of the wave field.

So, we can say that the nature of filament formation is more dependent on the kind of pump that is applied to the KAW wavepacket. These filamentary structures act as a faster way to transfer energy from large scales on the order of ion acoustic gyroradius to small scales on the order of electron thermal gyroradius. The inhomogeneities in magnetic field and density in the form of perturbation in our simulation take energy from the main KAW by nonlinear interaction and it forms coherent structures when the waves propagate. Gershman et al. (2017) estimated the modeled wave growth rates of KAWs and found that the local generation of observed KAWs (as observed by NASA's *Magnetospheric Multiscale (MMS)* mission) is not due to the local spatial gradients of plasma density. These are combined effects of nonlinearities arising from inhomogeneities in the field and density as well as other parametric forcing (e.g. magnetopause motion). When these nonlinear interactions are combined with the imbalance in the number of particles moving faster than the wave, plasma heating occurs (Gershman et al. 2017).

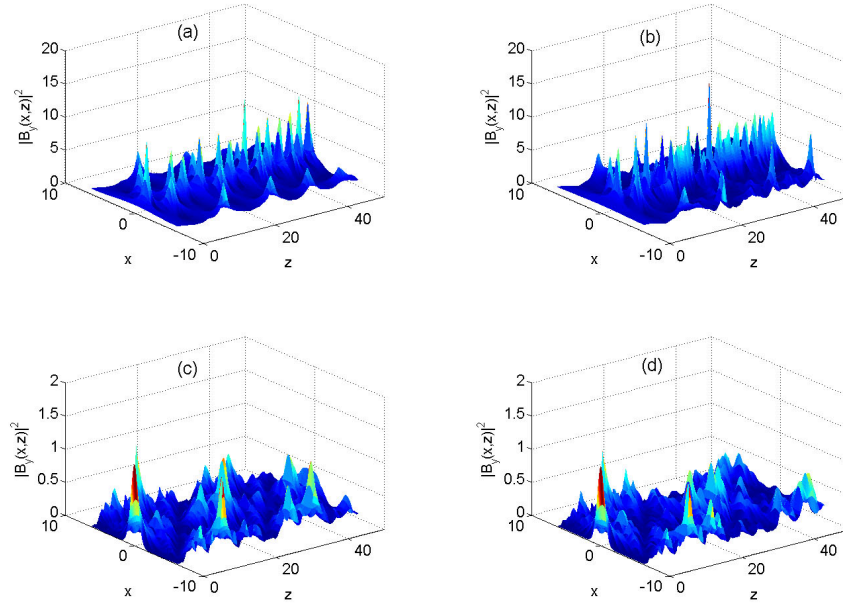


**Fig. 1** 2D-spatial profile of magnetic field intensity for solar wind at 1 AU: (a) IC-1, (b) IC-2, (c) IC-3 and (d) IC-4.

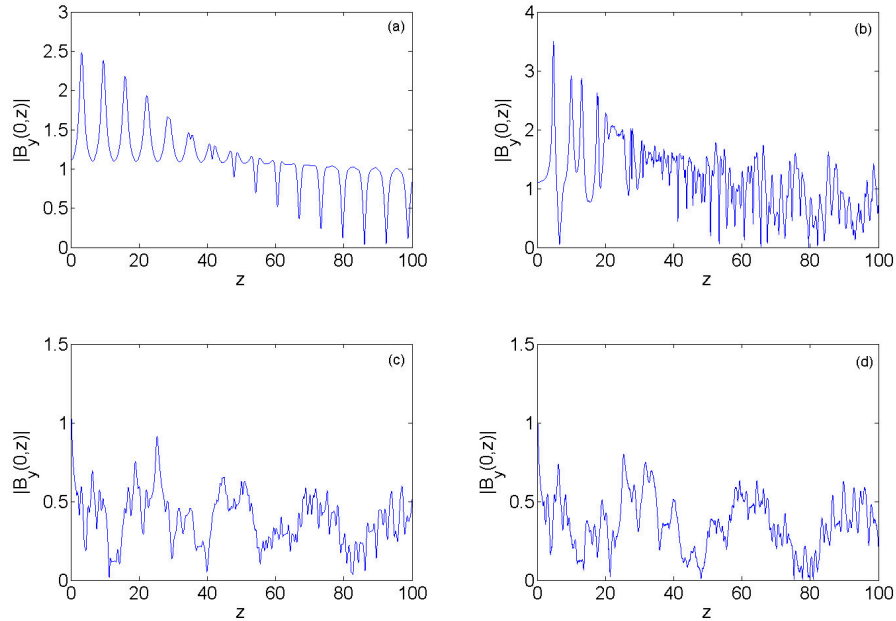


**Fig. 2** The variation of magnetic field amplitude with the distance of propagation for (a) IC-1, (b) IC-2, (c) IC-3 and (d) IC-4.

In nonlinear KAWs, parallel fluctuations in fields and current density can be sufficiently large in amplitude so that they can trap electrons in between the wave packets. The fluctuations in parallel magnetic field give rise to transitory time damping effects which are the magnetic analog of Landau damping. It is evident from Figure 1

that when the magnetic field intensity is high enough, it leads to breaking the coherent structures and triggering kinetic scales of KAWs, thereby heating the plasma particles. The ion motions decouple from the electron motions when these filamentary sizes are smaller than that of the ion acoustic gyroradius  $\rho_s$ . Here from the figure, the large

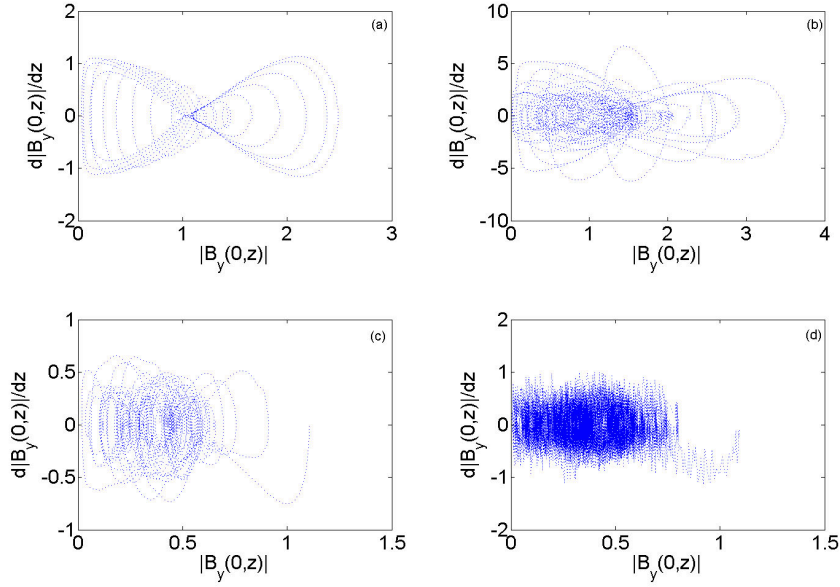


**Fig. 3** Phase space plots of KAWs for (a) IC-1, (b) IC-2, (c) IC-3 and (d) IC-4.

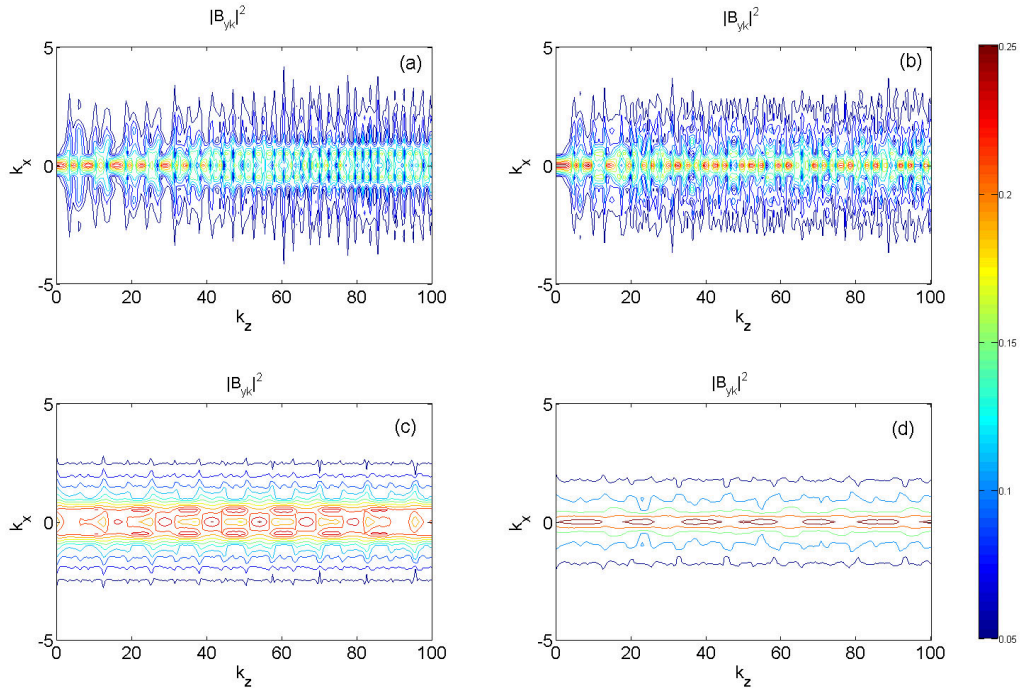


**Fig. 4** Contours of  $|B_{yk}|^2$  in  $k_x, k_z$  Fourier modes for solar wind at 1 AU: (a) IC-1, (b) IC-2, (c) IC-3 and (d) IC-4.

transverse filament sizes are on the order of ion gyroradius  $\approx 6\rho_s = 188.50$  km at half of the peak intensity. While investigating the coherent formation and spectral turbulence, Lion et al. (2016) found the radius of the Alfvénic vortex with highest intensity to be  $8\rho_s$  at half of the intensity peak. In studying the Alfvén vortex, Chmyrev et al. (1988)

observed the transverse scale of filaments to be on the order of  $\rho_s$ . If we increase the pump wave amplitude which can be achieved by increasing the parameter  $g$  as carried out by Sharma et al. (2006), the filamentary size becomes less than  $\rho_s$ . When the short perpendicular wavelength is comparable to the microscale kinetic scales of the particles

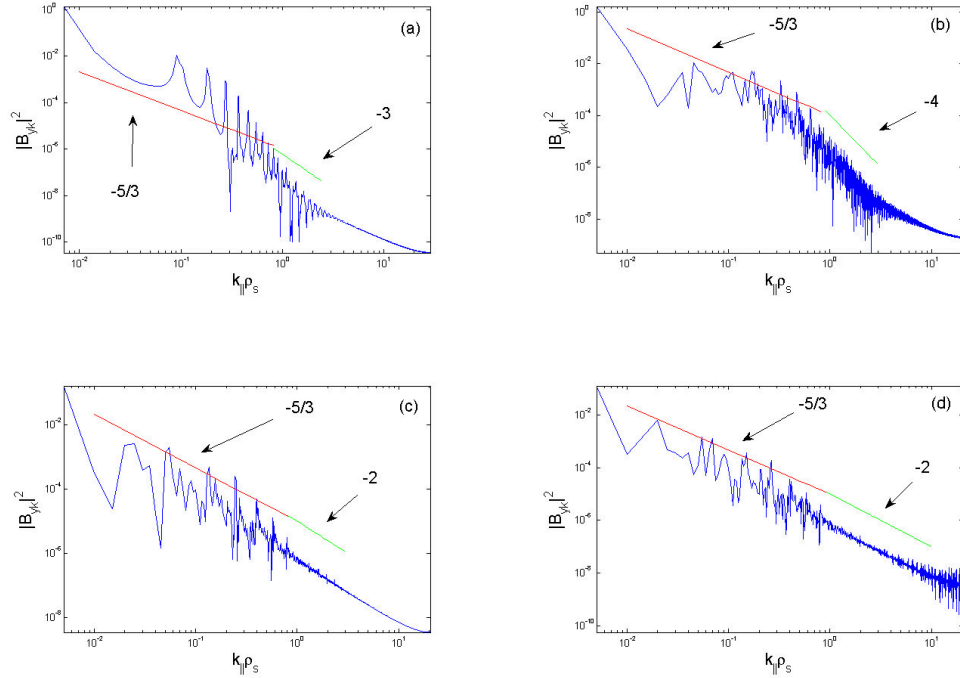


**Fig. 5** Magnetic field spectral intensity  $|B_{yk}|^2$  versus  $k_{\parallel}\rho_s$  for solar wind at 1 AU: (a) IC-1, (b) IC-2, (c) IC-3 and (d) IC-4.

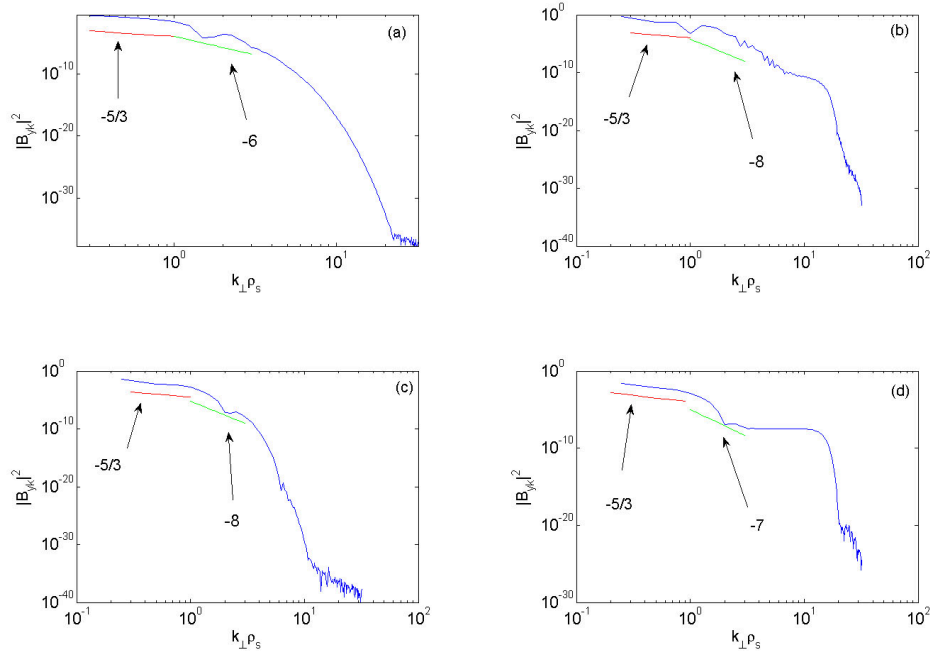


**Fig. 6** Magnetic field spectral intensity  $|B_{yk}|^2$  against  $k_{\perp}\rho_s$  for solar wind at 1 AU: (a) IC-1, (b) IC-2, (c) IC-3 and (d) IC-4.

such as  $\rho_s$ , the transfer of energy from the KAW to particles in the plasma is effective.

In order to understand the magnetic field propagation in space, we carried out further diagnostics by taking the

magnetic field amplitude at a fixed distance in the transverse direction  $x(x = 0)$  described as  $B_y(0, z)$ . Figure 2 depicts the propagation of field amplitudes with different initial conditions. The motion appears to be quasiperi-

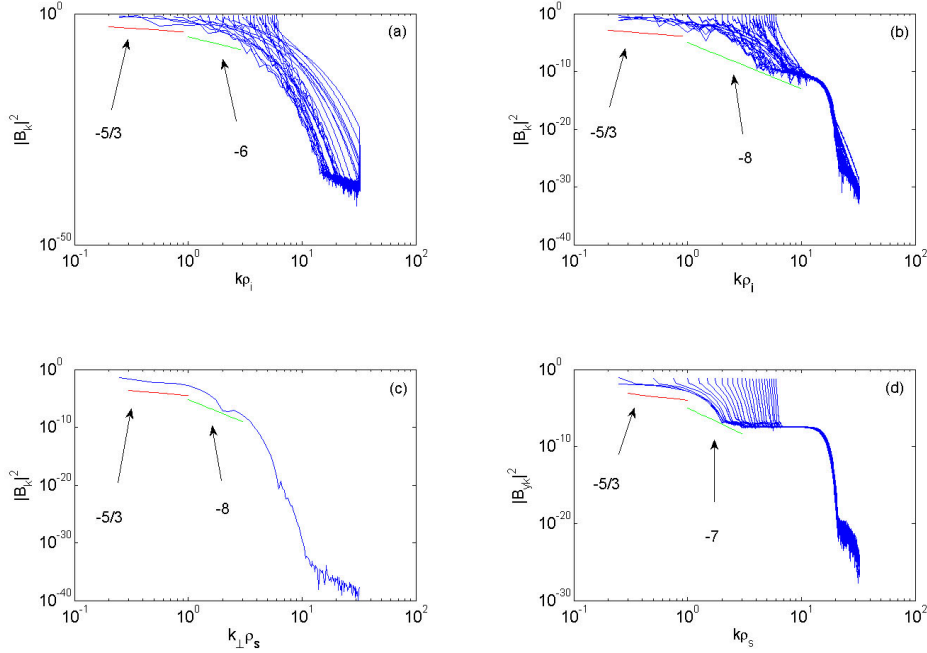


**Fig. 7** Magnetic field spectral intensity  $|B_{yk}|^2$  versus  $k\rho_s$  for solar wind at 1 AU: (a) IC-1, (b) IC-2, (c) IC-3 and (d) IC-4.

odic for IC-1, but for other initial conditions it tends to chaotic behavior. We constructed the phase space portraits by plotting  $|B_y(0, z)|$  vs.  $d|B_y(0, z)|/dz$  in Figure 3. It is evident that for IC-1 (Fig. 3(a)) the motion follows an irregular homoclinic orbit (HMO) with a finite number of dots. The hyperbolic fixed point was observed at  $|B_{y0}| = \sqrt{\ln(1-2g)/2g}$ . The motion is undergoing a quasiperiodic oscillation. For other initial conditions, the orbits have an infinite number of dots without any regular fixed point, filling up substantial portions of the space. So, the dynamics of the KAW coherent structure formation are spatially chaotic.

From the above results, we have seen that for all four kinds of initial conditions, some features of chaotic motion exist. To investigate this quantitatively, we calculated the Lyapunov exponent for all initial conditions as,

$$\lambda = \lim_{z \rightarrow \infty} \lim_{b(z=0) \rightarrow 0} \left\{ \frac{1}{z} \ln \left| \frac{b(z)}{b(z=0)} \right| \right\}, \quad (22)$$

where  $b$  is the first derivative of  $B(x, z)$  with respect to  $z$  at a fixed  $x$ . For IC-1, IC-2, IC-3 and IC-4, the Lyapunov exponents were found to be 0.013, 0.028, 0.052 and 0.097 respectively. The positive Lyapunov exponents for all four cases definitely show that the system is complex and spatially chaotic. Therefore, the KAW propagation and its distribution of energy depend on the initial profile of the inhomogeneous magnetic field.

Next, we study the propagation of energy in Fourier space. For that purpose we generate the contour plots of  $|B_{yk}|^2$  in the  $k_x, k_z$  plane (Fig. 4). In this plot, the lines connect the coordinates of  $k_x$  and  $k_z$  having the same values of  $|B_{yk}|^2$ . The color bar displayed in the right panel of the graph represents the intensity of the magnetic field. The figure illustrates that most of the energy is confined initially at  $k_x = 0$ . In the case of IC-1 and IC-2, the initial energy localized at  $k_x = 0$  is distributed to higher  $k_x$  after propagating a small distance in the  $z$  direction, i.e. at  $k_z \approx 3.5$ . The distribution of energy at transverse wavenumber ( $k_x = k_\perp$ ) is more evident in IC-1 in comparison to IC-2. In IC-3 and IC-4, the energy is already distributed from the initial distance, i.e.,  $k_z = 0$ .

Next we studied the transfer of energy in wavenumber spectrum by plotting  $|B_{yk}|^2$  against  $k_z = k_\parallel$  (Fig. 5(a)-5(d)). In the early studies of weak MHD turbulence through nonlinear interaction among the three counter-propagating Alfvén waves, it was predicted that there was no cascade of energy in parallel wavenumber space (Kraichnan 1965; Shebalin et al. 1983). In the strong turbulence MHD regime, the nonlinear term arises from all orders, not only by three wave interactions, thereby leading to the cascade of energy in the parallel wavenumber space (Goldreich & Sridhar 1995). For all the initial conditions with  $k_\parallel\rho_s < 1$ , i.e. in the inertial range, the spectral indices are of Kolmogorov scale  $k_\parallel^{-5/3}$  as observed by many au-

thors (Champeaux et al. 1998; Laveder et al. 2001; Sulem & Sulem 1999). However, there is a first spectral break at  $k_{\parallel}\rho_s \approx 1$  showing no fixed spectral slope. This is the transition region from inertial range (ion scale) to kinetic range (electron scale). In the transition region, evidence of a variable spectral power law has been demonstrated by many authors, for example, fixed power law by Smith et al. (2006) and Sahraoui et al. (2010); smooth transition without any power law by Bruno & Trenchi (2014); and positive slopes (Jian et al. 2014). Our spectral results also exhibit variable slopes at the transition region. Numerous investigations (Leamon et al. 1998; Bale et al. 2005; Smith et al. 2006; Sahraoui et al. 2009, 2013; Roberts et al. 2013) reported having a steeper spectral index ( $k^{-2}$  to  $k^{-5.5}$ ) after the transition range at ion kinetic scale ( $k\rho_s > 1$ ). In our Figure 5, these slopes are  $-3$ ,  $-4$ ,  $-2$  and  $-2$  for IC-1, IC-2, IC-3 and IC-4 respectively.

In order to gain a detailed understanding about energy exchange between the various Fourier modes, especially to transverse wavenumber  $k_x = k_{\perp}$ , we plotted the log-log scale of  $|B_{yk}|^2$  versus  $k_{\perp}\rho_s$  in Figure 6(a)–(d). At the inertial scale ( $k_{\perp}\rho_s < 1$ ), it follows the usual Kolmogorov scale of  $-5/3$  spectral index. At scales smaller than the ion scale (i.e.  $k_{\perp}\rho_s > 1$ ), the spectral indices from Figure 6 are  $-6$  for IC-1,  $-8$  for IC-2 and IC-3, and  $-7$  for IC-4. On the electron scale, i.e.,  $k_{\perp}\rho_s \geq 10$  or  $k_{\perp}\rho_e \approx 1$ , the spectral indices are deeper.

At the scale length of electron inertial length, i.e.,  $k_{\perp}\rho_s \approx 10$ , a second break point in the spectral index occurs. Below this scale length, our present model is not applicable since  $\omega < \omega_{ci}$ . By analyzing the *Cluster* spacecraft data, Sahraoui et al. (2009) showed that the cascade of energy is carried by KAWs with  $\omega < \omega_{ci}$  down to  $k_{\perp}\rho_i \approx 20$ , corresponding to frequency of around 5 Hz and reaching the noise level of the instrument. Therefore, in our study no conclusion can be drawn for this deep range of spectral index beyond  $k_{\perp}\rho_s \approx 10$ . In this regime, whistler waves ( $\omega > \omega_{ci}$ ) or the interaction of KAWs with whistler waves is more relevant to explain the phenomena.

In the kinetic small scale regime, many authors (Chen et al. 2010; Sahraoui et al. 2010; Narita et al. 2011) demonstrated that the magnetic fluctuations are anisotropic with respect to the mean magnetic field. It was also found that the turbulence is more anisotropic at large wavenumbers, so that energy is cascaded more in the transverse wavenumber where  $k_{\perp} > k_{\parallel}$ . In our results also, by examining Figure 6, we found that the magnetic spectral slope in the kinetic small scale is deeper along  $k_{\perp}$  in comparison to along  $k_{\parallel}$  from Figure 5. The slopes along  $k_{\perp}$  are

$-6$ ,  $-8$ ,  $-8$  and  $-7$  for IC-1, IC-2, IC-3 and IC-4 respectively. So, the spectral energy redistribution via the perpendicular wavenumber is dependent upon the nature of the pump KAW and the magnetic field fluctuations in the wavenumber domain. The *Cluster* observations analyzed by Sahraoui et al. (2013) imply the existence of spectral indices ranging from  $-5.5$  to  $-3.5$  with a broad spectrum at the electron scales.

The last magnetic spectra presented (Fig. 7) are  $|B_{yk}|^2$  versus  $k\rho_s$  where  $k = \sqrt{k_{\parallel}^2 + k_{\perp}^2}$  manifests a slope of  $-6$  to  $-8$  at  $k\rho_s > 1$ . By studying the data from *Cluster* spacecrafts, Alexandrova et al. (2009) indicated that the spectral break is fitted with  $\sim e^{-\sqrt{k\rho_e}}$  for the range of  $k\rho_e$  from 0.1 to 1. There are several explanations for this steeper range of spectral range at the dissipation region. According to Howes et al. (2006) and Schekochihin et al. (2009), the steepening of spectral index may be because of non-dispersive Alfvén waves becoming dispersive KAWs. When the scales are close to ion gyroradius or electron inertial length, strong Landau damping happens in KAW via wave particle interactions (Gary & Nishimura 2004; Sahraoui et al. 2009). Because of having similar properties between whistler waves and KAWs as well as the difficulties in distinguishing between them, it is unclear and remains an open issue whether the small scale fluctuations are due to KAWs or whistler waves, or the interactions between them (Gary & Smith 2009; Salem et al. 2012; Boldyrev et al. 2013; Chen et al. 2013b). The other possible processes are interactions of other waves such as ion acoustic and magnetosonic waves with KAWs via the nonlinearity that arises from the ponderomotive forces. Therefore, it remains undecided which of these or combinations give a satisfactory reason for steep kinetic range spectra.

It should be mentioned here that our present study is limited to the steady state (spatial domain) only whereas in reality, fluctuations in the solar wind are dependent on both space and time. Therefore, we are planning to extend the present work to the transient case, which includes spatial and temporal dependences together.

## 4 CONCLUSIONS

We have studied the numerical simulation of the dynamical equation satisfied by KAWs by including inhomogeneity in transverse magnetic field and density fluctuations at 1 AU solar wind parameters. The coherent structures of KAWs with high intensity are formed and they are dependent on the type of fluctuations that were represented

by our four different initial conditions in the simulation. It was found that the perturbation present in the magnetic field may lead to forming these coherent structures via taking energy from the pump KAWs. When there is a balance between the diffraction term and nonlinearity arising from the plasma inhomogeneity profile, spatially solitary (coherent) structures are formed. The imbalance of these two leads to collapse of the KAW packets and transfer of energy from the wave to the particles in the plasma. This transfer of energy at perpendicular wavevector is more for uniform initial pump KAW (IC-1 and IC-2) rather than those for non-uniform initial pump wave from a Gaussian wavefront (IC-3 and IC-4). The transfer of energy at kinetically small scales when the wavenumber is less than the ion gyroradius and comparable to electron inertial length causes solar wind turbulence and heating of the plasma. In our study, we found the spectral index following the Kolmogorov scale of  $-5/3$  which is in the inertial range followed by deeper indices varying from  $-2.5$  to  $-8$  in the kinetic dissipation range.

In the magnetized solar wind, since the number of particles is very low, their mean free path is of the order of 1 AU. Therefore, the collisions among particles are very rare and the scale length of the dissipation process is not precisely defined. In the turbulent state of the solar wind, there are several spatial characteristic scale lengths, such as  $\rho_s$ ,  $\rho_i$ ,  $\lambda_i$ ,  $\rho_e$  and  $\lambda_e$ . At these scale lengths, the physical mechanisms responsible for energy transfer change, giving different energy transfer rates. It leads to a change in the energy spectral shapes. Since the localization process is a faster way to transport energy, the dependence of initial conditions of fluctuations on the localization of Alfvénic coherent structures may provide clues to study and understand the phenomenon of dissipation in the solar wind.

**Acknowledgements** Bheem Singh Jatav is grateful to UGC for providing RGNF for doing research work.

## References

- Alexandrova, O., Carbone, V., Veltri, P., & Sorriso-Valvo, L. 2008, *ApJ*, 674, 1153
- Alexandrova, O., Saur, J., Lacombe, C., et al. 2009, *Physical Review Letters*, 103, 165003
- Alexandrova, O., Lacombe, C., Mangeney, A., Grappin, R., & Maksimovic, M. 2012, *ApJ*, 760, 121
- Bale, S. D., Kellogg, P. J., Mozer, F. S., Horbury, T. S., & Reme, H. 2005, *Physical Review Letters*, 94, 215002
- Bavassano, B., Pietropaolo, E., & Bruno, R. 1998, *J. Geophys. Res.*, 103, 6521
- Bellan, P. M., & Stasiewicz, K. 1998, *Physical Review Letters*, 80, 3523
- Boldyrev, S., & Perez, J. C. 2012, *ApJ*, 758, L44
- Boldyrev, S., Horaites, K., Xia, Q., & Perez, J. C. 2013, *ApJ*, 777, 41
- Bruno, R., & Carbone, V. 2013, *Living Reviews in Solar Physics*, 10, 2
- Bruno, R., & Trenchi, L. 2014, *ApJ*, 787, L24
- Champeaux, S., Passot, T., & Sulem, P. L. 1998, *Physics of Plasmas*, 5, 100
- Chang, O., Gary, S. P., & Wang, J. 2013, *Journal of Geophysical Research (Space Physics)*, 118, 2824
- Chaston, C. C., Bonnell, J. W., Carlson, C. W., et al. 2003, *Journal of Geophysical Research (Space Physics)*, 108, 8003
- Chaston, C. C., Bonnell, J. W., Carlson, C. W., et al. 2004, *Journal of Geophysical Research (Space Physics)*, 109, A04205
- Chaston, C. C., Phan, T. D., Bonnell, J. W., et al. 2005a, *Physical Review Letters*, 95, 065002
- Chaston, C. C., Peticolas, L. M., Carlson, C. W., et al. 2005b, *Journal of Geophysical Research (Space Physics)*, 110, A02211
- Chen, H.-H., & Liu, C.-S. 1976, *Physical Review Letters*, 37, 693
- Chen, L., & Wu, D. J. 2010, *Physics of Plasmas*, 17, 062107
- Chen, C. H. K., Horbury, T. S., Schekochihin, A. A., et al. 2010, *Physical Review Letters*, 104, 255002
- Chen, L., Wu, D. J., & Hua, Y. P. 2011, *Phys. Rev. E*, 84, 046406
- Chen, L., & Wu, D. J. 2012, *ApJ*, 754, 123
- Chen, C. H. K., Boldyrev, S., Xia, Q., & Perez, J. C. 2013a, *Physical Review Letters*, 110, 225002
- Chen, L., Wu, D. J., & Huang, J. 2013b, *Journal of Geophysical Research (Space Physics)*, 118, 2951
- Chen, C. H. K., Leung, L., Boldyrev, S., Maruca, B. A., & Bale, S. D. 2014, *Geophys. Res. Lett.*, 41, 8081
- Chen, L., Wu, D. J., Zhao, G. Q., Tang, J. F., & Huang, J. 2015, *Journal of Geophysical Research (Space Physics)*, 120, 61
- Chmyrev, V. M., Bilichenko, S. V., Pokhotelov, O. A., et al. 1988, *Phys. Scr*, 38, 841
- Cranmer, S. R., Field, G. B., & Kohl, J. L. 1999, *ApJ*, 518, 937
- Cravens, T. E. 2004, *Physics of Solar System Plasmas* (Cambridge, UK: Cambridge University Press)
- Duan, S.-p., & Li, Z.-y. 2005, *Chinese Astronomy and Astrophysics*, 29, 1
- Duan, S. P., Li, Z. Y., & Liu, Z. X. 2005, *Planet. Space Sci.*, 53, 1167
- Duan, S., Liu, Z., & Angelopoulos, V. 2012, *Chinese science bulletin*, 57, 1429
- Galtier, S. 2006, *J. Plasma Phys.*, 72, 721
- Gary, S. P. 1999, *J. Geophys. Res.*, 104, 6759
- Gary, S. P., & Nishimura, K. 2004, *Journal of Geophysical Research (Space Physics)*, 109, A02109
- Gary, S. P., & Smith, C. W. 2009, *Journal of Geophysical Research (Space Physics)*, 114, A12105

- Gekelman, W., Pribyl, P., Palmer, N., Vincena, S., Mitchell, C. 1999, *Bull Am. Phys. Soc.*, 44, 71
- Gershman, D. J., F-Viñas, A., Dorelli, J. C., et al. 2017, *Nature Communications*, 8, 14719
- Goldreich, P., & Sridhar, S. 1995, *ApJ*, 438, 763
- Goldstein, M. L., Roberts, D. A., & Fitch, C. A. 1994, *J. Geophys. Res.*, 99, 11519
- Hasegawa, A., & Chen, L. 1975, *Physical Review Letters*, 35, 370
- He, J., Marsch, E., Tu, C., Yao, S., & Tian, H. 2011, *ApJ*, 731, 85
- Horbury, T. S., Balogh, A., Forsyth, R. J., & Smith, E. J. 1996, *A&A*, 316, 333
- Howes, G. G. 2009, *Nonlinear Processes in Geophysics*, 16, 219
- Howes, G. G., Cowley, S. C., Dorland, W., et al. 2006, *ApJ*, 651, 590
- Howes, G. G., Dorland, W., Cowley, S. C., et al. 2008a, *Physical Review Letters*, 100, 065004
- Howes, G. G., Cowley, S. C., Dorland, W., et al. 2008b, *Journal of Geophysical Research (Space Physics)*, 113, A05103
- Howes, G. G., Cowley, S. C., Dorland, W., et al. 2008c, *Physical Review Letters*, 101, 149502
- Howes, G. G., Tenbarger, J. M., & Dorland, W. 2011a, *Physics of Plasmas*, 18, 102305
- Howes, G. G., Tenbarger, J. M., Dorland, W., et al. 2011b, *Physical Review Letters*, 107, 035004
- Jian, L. K., Wei, H. Y., Russell, C. T., et al. 2014, *ApJ*, 786, 123
- Kraichnan, R. H. 1965, *Physics of Fluids*, 8, 1385
- Kruer, W. 2003, *The Physics of Laser Plasma Interactions* (Boulder, CO)
- Laveder, D., Passot, T., & Sulem, P. L. 2001, *Physica D Nonlinear Phenomena*, 152, 694
- Leamon, R. J., Smith, C. W., Ness, N. F., Matthaeus, W. H., & Wong, H. K. 1998, *J. Geophys. Res.*, 103, 4775
- Leamon, R. J., Matthaeus, W. H., Smith, C. W., et al. 2000, *ApJ*, 537, 1054
- Lee, L. C., Johnson, J. R., & Ma, Z. W. 1994, *J. Geophys. Res.*, 99, 17405
- Li, H., Wang, C., Chao, J., & Hsieh, W. 2016, *Journal of Geophysical Research: Space Physics*, 121, 42
- Lion, S., Alexandrova, O., & Zaslavsky, A. 2016, *ApJ*, 824, 47
- Liu, Z.-X., He, J.-S., & Yan, L.-M. 2014, *RAA (Research in Astronomy and Astrophysics)*, 14, 299
- Malovichko, P. P. 2008, *Kinematics and Physics of Celestial Bodies*, 24, 236
- Markovskii, S. A., Vasquez, B. J., & Smith, C. W. 2008, *ApJ*, 675, 1576
- Marsch, E., & Tu, C.-Y. 1990, *J. Geophys. Res.*, 95, 8211
- Marsch, E., & Tu, C.-Y. 2001, *J. Geophys. Res.*, 106, 227
- Matthaeus, W. H., Goldstein, M. L., & Smith, C. 1982, *Physical Review Letters*, 48, 1256
- Narita, Y., Gary, S. P., Saito, S., Glassmeier, K.-H., & Motschmann, U. 2011, *Geophys. Res. Lett.*, 38, L05101
- Neugebauer, M. 2004, *Journal of Geophysical Research (Space Physics)*, 109, A02101
- Osman, K. T., Matthaeus, W. H., Greco, A., & Servidio, S. 2011, *ApJ*, 727, L11
- Perri, S., Carbone, V., & Veltri, P. 2010, *ApJ*, 725, L52
- Podesta, J. J. 2013, *Sol. Phys.*, 286, 529
- Podesta, J. J., Borovsky, J. E., & Gary, S. P. 2010, *ApJ*, 712, 685
- Roberts, O. W., Li, X., & Li, B. 2013, *ApJ*, 769, 58
- Sahraoui, F., Goldstein, M. L., Robert, P., & Khotyaintsev, Y. V. 2009, *Physical Review Letters*, 102, 231102
- Sahraoui, F., Goldstein, M. L., Belmont, G., Canu, P., & Rezeau, L. 2010, *Physical Review Letters*, 105, 131101
- Sahraoui, F., Belmont, G., & Goldstein, M. L. 2012, *ApJ*, 748, 100
- Sahraoui, F., Huang, S. Y., Belmont, G., et al. 2013, *ApJ*, 777, 15
- Saito, S., Gary, S. P., & Narita, Y. 2010, *Physics of Plasmas*, 17, 122316
- Salem, C. S., Howes, G. G., Sundkvist, D., et al. 2012, *ApJ*, 745, L9
- Savin, S. P., Romanov, S. A., Fedorov, A. O., et al. 1998, *Geophys. Res. Lett.*, 25, 2963
- Schekochihin, A. A., Cowley, S. C., Dorland, W., et al. 2008, *Plasma Physics and Controlled Fusion*, 50, 124024
- Schekochihin, A. A., Cowley, S. C., Dorland, W., et al. 2009, *ApJS*, 182, 310
- Sergeev, V. A., Sauvaud, J.-A., Popescu, D., et al. 2000, *Geophys. Res. Lett.*, 27, 851
- Shaikh, D. 2010, *MNRAS*, 405, 2521
- Sharma, R. P., Singh, H. D., & Malik, M. 2006, *Journal of Geophysical Research (Space Physics)*, 111, A12108
- Shebalin, J. V., Matthaeus, W. H., & Montgomery, D. 1983, *Journal of Plasma Physics*, 29, 525
- Shukla, P. K., & Stenflo, L. 1999, *Physics of Plasmas*, 6, 4120
- Shukla, P. K., Stenflo, L., & Bingham, R. 1999, *Physics of Plasmas*, 6, 1677
- Shukla, P. K., & Stenflo, L. 2000a, *Physics of Plasmas*, 7, 2738
- Shukla, P. K., & Stenflo, L. 2000b, *Physics of Plasmas*, 7, 2747
- Shukla, P. K., & Stenflo, L. 2005, *Physics of Plasmas*, 12, 084502
- Siversky, T., Voitenko, Y., & Goossens, M. 2005, *Space Sci. Rev.*, 121, 343
- Smith, C. W., Hamilton, K., Vasquez, B. J., & Leamon, R. J. 2006, *ApJ*, 645, L85
- Sulem, C., & Sulem, P.-L. 1999, *Applied Mathematical Sciences*, 139
- Sundkvist, D., Retinò, A., Vaivads, A., & Bale, S. D. 2007, *Physical Review Letters*, 99, 025004
- Tsiklauri, D. 2011, *Physics of Plasmas*, 18, 092903
- Tsiklauri, D. 2012, *Physics of Plasmas*, 19, 082903
- Tsurutani, B. T., Smith, E. J., Anderson, R. R., et al. 1982, *J. Geophys. Res.*, 87, 6060
- Tu, C.-Y., Marsch, E., & Rosenbauer, H. 1990, *Geophys. Res. Lett.*, 17, 283
- Tu, C.-Y., & Marsch, E. 1993, *J. Geophys. Res.*, 98, 1257

- Tu, C.-Y., & Marsch, E. 1995, *Space Sci. Rev.*, 73, 1  
Voitenko, Y., & Goossens, M. 2004, *ApJ*, 605, L149  
Wang, X., He, J., Tu, C., et al. 2012, *ApJ*, 746, 147  
Winterhalter, D., Neugebauer, M., Goldstein, B. E., et al. 1994, *J. Geophys. Res.*, 99, 23371  
Wu, D. J. 2003, *Physics of Plasmas*, 10, 1364  
Wu, D. J., & Fang, C. 2003, *ApJ*, 596, 656  
Wu, D. J., & Chao, J. K. 2004, *Journal of Geophysical Research (Space Physics)*, 109, A06211  
Wu, D. J., & Yang, L. 2006, *A&A*, 452, L7  
Wu, D. J., & Chen, L. 2013, *ApJ*, 771, 3  
Wygant, J. R., Keiling, A., Cattell, C. A., et al. 2002, *Journal of Geophysical Research (Space Physics)*, 107, 1201  
Xu, T., Tian, B., Li, L.-L., Lü, X., & Zhang, C. 2008, *Physics of Plasmas*, 15, 102307  
Yoon, P. H. 1995, *Physica Scripta*, 60, 127  
Zhou, C., He, X. T., & Chen, S. 1992, *Phys. Rev. A*, 46, 2277  
Zhou, C., & He, X. T. 1994, *Phys. Rev. E*, 49, 4417